arXiv:1411.5055v1 [astro-ph.GA] 18 Nov 2014

HD/H_2 as a probe of the roles of gas, dust, light, metallicity and cosmic rays in promoting the growth of molecular hydrogen in the diffuse interstellar medium

H. S. Liszt
National Radio Astronomy Observatory
520 Edgemont Road, Charlottesville, VA, 22903-2475
hliszt@nrao.edu

ABSTRACT

We modelled recent observations of UV absorption of HD and H_2 in the Milky Way and toward damped/sub-damped Lyman alpha systems at z=0.18 and z > 1.7. N(HD)/N(H_2) ratios reflect the separate self-shieldings of HD and H_2 and the coupling introduced by deuteration chemistry. Locally, observations are explained by diffuse molecular gas with 16 cm^{-3} $\lesssim$ n(H) $\lesssim$ 128 cm^{-3} if the cosmic-ray ionization rate per H-nucleus $\zeta_H = 2\times10^{-16}$ s^{-1} as inferred from H_3^+ and OH^+. The dominant influence on N(HD)/N(H_2) is the cosmic-ray ionization rate with a much weaker downward dependence on n(H) at Solar metallicity, but dust-extinction can drive N(HD) higher as with N(H_2). At z > 1.7, N(HD) is comparable to the Galaxy but with 10x smaller N(H_2) and somewhat smaller N(H_2)/N(H I). Comparison of our Galaxy and the Magellanic Clouds shows that smaller H_2/H is expected at sub-Solar metallicity and we show by modelling that HD/H_2 increases with density at low metallicity, opposite to the Milky Way. Observations of HD would be explained with higher n(H) at low metallicity but high-z systems have high HD/H_2 at metallicity 0.04 $\lesssim$ Z $\lesssim$ 2 Solar. In parallel we trace dust-extinction and self-shielding effects. The abrupt H_2 transition to H_2/H $\approx$ 1-10% occurs mostly from self-shielding although it is assisted by extinction for n(H) $\lesssim$ 16 cm^{-3}. Interior H_2 fractions are substantially increased by dust extinction below $\lesssim$ 32 cm^{-3}. At smaller n(H), ζ_H, small increases in H_2 triggered by dust extinction can trigger abrupt increases in N(HD).

Subject headings: astrochemistry . ISM: molecules . ISM: clouds. Galaxy

1. Introduction

Like molecular hydrogen H_2, the much rarer deuterated isotopologue HD has been studied and observed across cosmic time. A survey of HD/H_2 ratios along 41 galactic sightlines has recently been published by Snow et al. (2008), revising and greatly extending the work of Lacour et al. (2005) and yet-earlier results summarized by Liszt (2003). Oliveira et al. (2014) recently detected HD in a low-redshift, low-metallicity Damped Lyman Alpha (DLA) system with column densities N(HD) and N(H_2) very much like those seen in the Milky Way. HD and H_2 have also been detected at eight redshifts toward six DLA and sub-DLA systems at z > 1.7 with N(HD)/N(H_2) ratios well above those seen in the Milky Way (Noterdaeme et al. 2008; Balashev et al. 2010; Ivanchik et al. 2010; Noterdaeme et al. 2010; Tumlinson et al. 2010).

The chemistry of deuterium and HD plays a special role in the formation of structure and the first stars in the early Universe (Gay et al. 2011). Although it is generally understood now that observations of HD can not provide a direct determination of the elemental [D/H] ratio (Le Petit et al. 2002; Snow et al. 2008; Ivanchik et al. 2010), [D/H] is well-determined by other means, with [D/H] = 2.54×10^{-5} in primordial gas (Pettini & Cooke 2012; Cooke et al. 2014) and [D/H] = 2.35×10^{-5} locally (Linsky et al. 2006).

Given that the intrinsic [D/H] ratio is reflected only indirectly in the HD/H_2 ratio, the study of HD is now of interest owing to its value as a probe of the microphysics of the diffuse atomic gas and the more general

problem of H_2-formation in relatively low-density diffuse neutral atomic gas. The formation rate of HD depends primarily on the local proton (or deuteron) density and hence on the strength of penetrating hydrogen-ionizing radiation (usually the cosmic-ray ionization rate). In turn, the proton density is balanced by the processes whereby atomic ions recombine, basically via grain-assisted recombination mediated by the same small particles that heat the gas via the photoelectric effect (Draine & Sutin 1987; Bakes & Tielens 1994; Wolfire et al. 1995). The interaction of H^+ and D^+ with HD and H_2 to equilibrate the HD/H_2 ratio couples the microphysics and HD chemistry to the general H_2 formation problem, highlighting the separate roles of shielding of H_2 and HD by themselves and by dust extinction.

Here we discuss these observations of HD in the context of models of the coupled heating/cooling- H_2-HD- formation in diffuse neutral atomic gas. Section 2 discusses models of H_2 and HD formation and self-shielding in diffuse clouds. In Section 3 observations of HD in the Milky Way are discussed and compared with the model results, which are explored in some detail in Section 4 in order to separate the various physical and chemical processes involved. Section 5 discusses what is known observationally of the H I-H_2 transition [1] in diffuse gas in nearby systems having sub-Solar metallicity and Section 6 discusses the observations of H_2 and HD in high-redshift Damped Lyman Alpha Systems (DLA). Section 7 is a summary.

2. Model calculations

2.1. H_2 and HD formation and self-shielding

This work is an update of our earlier investigation of the formation of HD and H_3^+(Liszt 2003), revised to study the wealth of new observations of HD noted in the Introduction. As before (Liszt 2003, 2007) we model the formation of H_2 self-consistently in a spherical gas cloud of uniform density immersed in the average ambient, isotropic galactic radiation field, and we compute the local kinetic temperature T_K following the methods of Wolfire and his collaborators (Wolfire et al. 1995, 2003). The equations of chemical and thermal balance are solved iteratively over a model with 128 or more equi-spaced radial shells, computing the radiation field in each shell averaged over the sur-

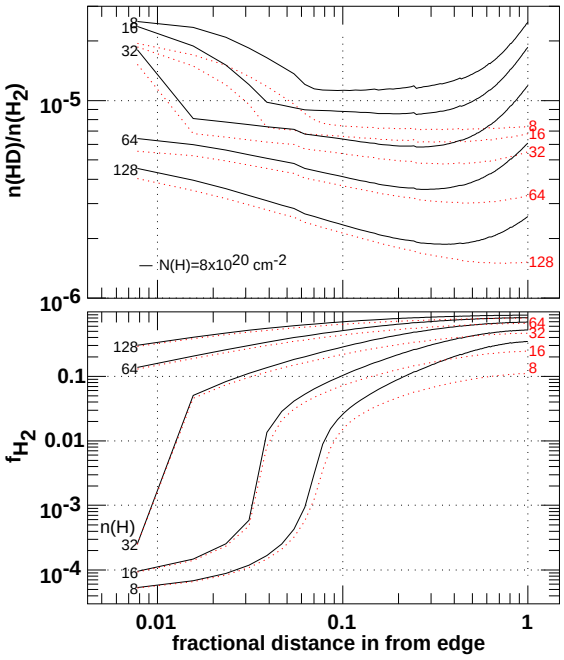

Fig. 2.— Radial variation of the H_2-fraction (lower panel) and HD/H_2 ratio (upper panel) for models with N(H) = 8×10^{20} cm^{-2} and number density n(H) = 8, 16, 32, 64 and 128 cm^{-3}. Dotted (red) lines are results without dust extinction of dissociating photons.

[1] In this work we refer to neutral atomic hydrogen as H I following the usage of Savage et al. (1977)

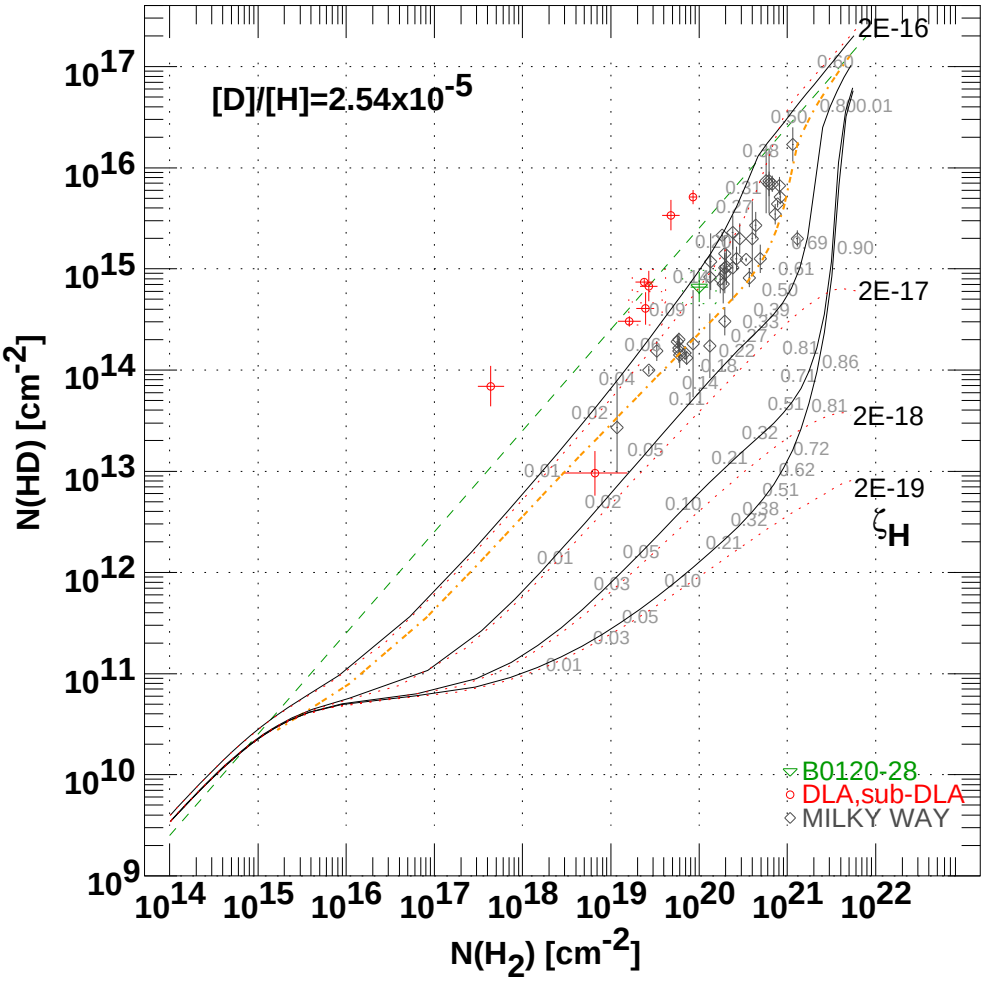

Fig. 1.— Observed and model HD and H_2 column densities for Milky Way sightlines from Snow et al. (2008) and Damped and sub-Damped Lyman Alpha systems (DLA) at z = 0.18 (B0120-28) and > 1.7. The solid black lines are calculated through the central line of sight toward uniform density gas spheres of total density n(H) = 16 cm^{-3} and primary cosmic ray ionization rates per H-atom 2×10^{-19} $s^{-1} \leq \zeta_H \leq 2\times10^{-16}$ s^{-1}. Numerical annotations show the H_2 fraction along the curves. The companion dotted lines show the results when the explicit shielding by dust extinction is neglected. The orange dashed-dotted line shows results for n(H) = 128 cm^{-3} and $\zeta_H = 2\times10^{-16}$ s^{-1} including dust extinction. The primordial ratio [D/H] = 2.54×10^{-5} (Pettini & Cooke 2012; Cooke et al. 2014) is shown as a green dashed line.

rounding 4π solid angle.

Following the prescription of Spitzer (1978) (see also Sternberg et al. (2014) the rate constant for H_2-formation on grain surfaces is taken as $R_G = 3 \times 10^{-18}$ cm^3 s^{-1} $\sqrt{T_K}$ but the thermal balance and temperature-dependent rate constant are not of crucial importance to the H_2-fraction. The same results are obtained using a fixed rate constant $R_G = 3.9 \times 10^{-17}$ cm^3 s^{-1} that is the average of the values obtained toward three stars by Gry et al. (2002) often cited in other work, as discussed in Section 5.2 (those sightlines are called out in Figure 5). The thermal balance is however very important to several endothermic reactions driving the oxygen and deuterium chemistry and to the overall ionization balance in the models.

The models described here differ from our previously published results in that they employ the H_2 photodissociation scheme of Draine & Bertoldi (1996) which explicitly treats dust attenuation of the radiation field at the wavelengths of the Lyman and Werner bands of H_2 (90 - 110 nm). The optical depth for dust absorption is $\tau_d = 1.9 \times 10^{-21}$N(H) (Draine 2003) as in Sternberg et al. (2014). Regarding our previous models based on the shielding factors of Lee et al. (1996), we note that incorporation of dust extinction is implicit and somewhat ambiguous in the formulation of Lee et al. (1996) where only an overall H_2 self-shielding function is employed, more similar to the earlier work of Federman et al. (1979).

The accuracy of the Draine & Bertoldi (1996) formulation was recently been verified in great detail by Sternberg et al. (2014) using an exact calculation in the context of the Meudon PDR code. Separation of dust extinction-related phenonema is important for understanding the HD formation problem, and perhaps even more important for understanding the general H_2-formation problem in media having low number density and/or low metallicity. The separate effects of dust extinction, and the shielding factors and dust extinctions for our models are explicitly shown and discussed here.

Direct HD formation on grains is modelled following the precepts of Le Petit et al. (2002) with a rate constant 40% larger than for H_2. This is manifest in the models shown in Figure 1 at very small N(H_2) but the direct formation of HD on grains is of almost no relevance to the observations of HD, as noted in Section 3. Self-shielding of HD is important in some cases, and may have contributed to the observed HD; the self-shielding of HD is the same function of N(HD) as the self-shielding of H_2 employing N(H_2) .

For reference, note that the cosmic-ray ionization rate of atomic hydrogen has been taken as $\zeta_H = 2 \times 10^{-16}$ s^{-1} as seems appropriate for the diffuse molecular ISM (McCall et al. 2002; Liszt 2003; Hollenbach et al. 2012; Indriolo et al. 2012). As a standard value we take $\Gamma_{H_2} = 4.3 \times 10^{-11}$ s^{-1} as the free-space photodissociation rate of H_2, as in the work of Draine & Bertoldi (1996) from which our H_2 self-shielding scheme was drawn.

Other values in the recent literature are $\Gamma_{H_2} = 2.5 \times 10^{-11}$ s^{-1} (over 2π steradians) in the work of Lee et al. (1996) and $\Gamma_{H_2} = 5.8 \times 10^{-11}$ s^{-1} in Sternberg et al. (2014). In this work, number and column densities implicitly refer to hydrogen nuclei when stated in the text, unless otherwise noted.

2.2. HD chemistry and the proton density

HD does not enjoy the high degree of self-shielding which is the *sine qua non* of high H_2-fractions. Hence the HD/H_2 ratio might be expected to be very small in diffuse gas, well below the inherent [D/H] ratio. That this is not so reflects the fractionation and charge exchange processes determined by the ambient proton and deuteron density as noted by Black & Dalgarno (1973), Watson (1973), Jura (1974), O'Donnell & Watson (1974) and Spitzer (1978).

The basic chemistry of H_2-HD interconversion has been sketched out by those authors and by Stancil et al. (1998) in the context of early-Universe chemistry; the rates used in this work were taken from Table 1 of Stancil et al. (1998). Although the fractionation/deuteration chemistry can be quite complex in cold, fully-molecularized dark clouds, it is fairly simple in warmer, lower-density diffuse regions where protons are abundant and only H_2 and HD need be considered, with exchange of protons or deuterons as the means of interconversion between the two molecular hydrogen isotopologues.

In a purely atomic gas ionized by cosmic rays the ionization and recombination rates of H and D atoms would be very nearly the same (the grain neutralization of D^+ is slower by a factor $\sqrt{2}$ owing to the smaller thermal speed of the twice-heavier deuterium isotope) but a strong and slightly endothermic charge exchange with protons $H^+ + D + \Delta E \rightarrow D^+ + H$ (rate constant $k_1 = 10^{-9}$ cm^3 s^{-1}, $\Delta E/k = 41$ K) tends to force n(D^+)/n(D I) $\approx$ n(H^+)/n(H I) exp(-41 K/T). In the presence of H_2

a rapid and relatively strongly exothermic reaction $D^+ + H_2 \rightarrow HD + H^+$ forms HD with rate constant $k_2 = 2.1 \times 10^{-9}$ cm^3 s^{-1}.

If only charge transfer and H_2 fractionation neutralize D^+ (a highly reductive assumption), a relatively compact expression gives the proton density n(p) required to reproduce a given HD/H_2 ratio in terms of observed quantities and physical constants, with no explicit dependence on either the density or recombination rates: we have

$$n(p) = \frac{n(HD)/n(H_2)}{[D/H]} \frac{\Gamma_{HD}}{k_2}[1+(\frac{k_2}{k_1}-2)\frac{n(H_2)}{n(H)}] \exp(\frac{41}{T}) \quad (1)$$

where n(H) = n(H I) + 2 n(H_2) and the photodissociation rate of HD in free space is $\Gamma_{HD} = \Gamma_{H_2} = 4.3 \times 10^{-11}$ s^{-1} (Draine & Bertoldi 1996; Le Petit et al. 2002). The required proton density n(p) derived from Eq. 1 is nearly independent of the molecular fraction in the gas for $k_2/k_1 = 2.1$ and there is no explicit dependence on density if the H_2 fraction is fixed. Of course the actual proton density may have quite strong dependence on n(H) and the assumptions used to derive Eq. 1 are rather archaic. Below we discuss the actual proton density in the models but the chief means by which an adequate proton density is achieved is the high default cosmic ray ionization rate that we have adopted, see Liszt (2003).

2.3. The D/H ratio

The models whose results are shown here use the cosmic ratio [D/H] = 2.54×10^{-5} (Pettini & Cooke 2012; Cooke et al. 2014) which is near the Milky Way value [D/H] = $2.35 \pm 0.24 \times 10^{-5}$ determined by Linsky et al. (2006). The actual gas phase [D/H] may be slightly smaller than the overall [D/H] value in the Milky Way but this is a small difference compared to the effects of the chemistry. Moreover the model results are intended to be generally relevant, for instance in Figure 1 where the local and high-z results are shown together.

3. Observations and models of HD in the Milky Way

3.1. Observations of HD

Shown in Figure 1 are the observational results for N(HD) and N(H_2) along the 41 Milky Way sightlines in the recent omnibus FUSE survey of Snow et al. (2008). Results for the DLA sightlines at z > 1.7 shown in Figure 1 are summarized in Table 1 and discussed in Section 6. Data for the low-z, low-metallicity DLA system at z=0.18 discussed by Oliveira et al. (2014) are also shown in Figure 1.

In a gas where H and D exist primarily as H_2 and HD, N(HD)/N(H_2) $\approx$ 2[D/H] $\approx 5 \times 10^{-5}$. In the opposite limit when only insignificant amounts of H and D are molecular, N(HD)/N(H_2) $\approx$ 1.4 [D/H] (Le Petit et al. 2002). By contrast the galactic HD column densities lie about a factor 10 below the cosmic [D/H] ratio in Fig. 1, falling nearly parallel to a line of constant N(HD)/N(H_2) = 3×10^{-6}. The regression analysis of Snow et al. (2008) found a power-law slope 1.25 ± 0.03. The N(HD)/N(H_2) values of Snow et al. (2008) are about three times larger than those considered in our simillar analysis of the same phenomena (Liszt 2003).

3.2. Comparison with models

The slightly super-linear empirical slope determined by Snow et al. (2008) means that N(HD)/N(H_2) increases with increasing molecular fraction f_{H_2} = 2N(H_2)/N(H) with N(H) = N(H I)+2N(H_2) (note the annotations in Fig. 1 showing f_{H_2} along the curves). Snow et al. (2008) pointed out that the models of Le Petit et al. (2002) seemed to predict the opposite behaviour except at $f_{H_2} \gtrsim 0.9$ and further noted that those models generally underpredicted N(HD) unless $f_{H_2} \lesssim 0.1$ or $f_{H_2} \gtrsim 0.9$. This was a straightforward consequence of the gas-phase chemistry of HD that segregated HD in regions of smaller density and lower H_2-fraction in diffuse clouds because of its dependence on the presence of a relatively high proton density.

Shown in Figure 1 are our equilibrium model results for sightlines through the centers of the uniform-density gas spheres discussed in Section 2. Results for a family of models with n(H) = 16 cm^{-3} and varying primary cosmic-ray ionization rate per H-atom 2×10^{-19} s^{-1} $\leq \zeta_H \leq 2 \times 10^{-16}$ s^{-1} are shown with and without the attenuation of Lyman and Werner Band photodissociating radiation by dust. Also shown are model results for n(H) = 128 cm^{-3}.

At the lowest cosmic-ray ionization rate considered, $\zeta_H = 2 \times 10^{-19}$ s^{-1}, the chemistry is essentially switched off and the predicted HD abundance is some three orders of magnitude below observed values. This demonstrates that when HD is seen in the Milky Way it overwhelmingly originates *in situ* in the gas phase

by deuteration of H_2. Although the actual [D/H] ratio in the gas phase is important, and n(D)/n(H) in the gas phase is affected by the n(HD)/n(H_2) ratio (Liszt 2006), considerations of HD formation on grains are irrelevant to HD-formation in the observed amounts. HD molecules formed on grains comprise a negligible fraction of the observed HD.

At the highest cosmic-ray ionization rate considered, $\zeta_H = 2\times10^{-16}$ s^{-1}, the observations are bounded by the models with n(H) = 16 cm^{-3} and 128 cm^{-3}. If the cosmic ray ionization rate is ubiquitous, the region occupied by the observations in Figure 1 is understood in terms of the relatively slow variations of the N(HD)/N(H_2) ratio with number density, and clouds with n(H) >> 128 cm^{-3} apparently were not sampled in the observations. Alternatively, if the cosmic ray ionization rate is assumed to vary, it should generally be in the sense of increasing above $\zeta_H = 2\times10^{-16}$ s^{-1}, implying somewhat higher number density, because neutral atomic gas with number density much below 16 cm^{-3} is not generally understood to be thermally stable in multi-phase models of the ISM , see e.g. Figure 7 of Wolfire et al. (2003).

Our models with $\zeta_H = 2\times10^{-16}$ s^{-1} and 16 cm^{-3} $\lesssim$ n(H) $\leq$ 128 cm^{-3} reproduce the observations, including the slightly super-linear slope derived by Snow et al. (2008), but the slope of the observed variation of N(HD) with N(H_2) must also reflect the underlying distribution of physical environments that were sampled. The HD column density results from a variety of influences including the gas-phase chemistry, the individual self-shielding of HD and H_2, their coupling via the chemistry, and the extinction of photodissociating UV radiation by dust. The consequential difference between our models and those of Le Petit et al. (2002) lies most nearly in the treatment of the overall ionization balance in the presence of grain-assisted recombination, which both allows and requires a higher cosmic ray ionization rate.

3.3. Cloud structure in f_{H_2} and n(HD)/n(H_2)

Although our models have uniform total number density n(H), the molecular fraction, proton density and n(HD)/n(H_2) ratio vary considerably within them. Figure 2 shows the n(HD)/n(H_2) ratio and molecular fraction as functions of radius for models with N(H) = 8×10^{20} cm^{-2} having column densities N(HD) and N(H_2) that are typical of the Milky Way data shown in Figure 1.

The models have 128 radial shells but only barely resolve some sharp variations near the outer cloud edges. Typical variations in n(HD)/n(H_2) are a factor two or three with higher values at the edge and center. At the highest density, n(H) = 128 cm^{-3}, the H_2-fraction varies less and generally in the opposite sense from n(HD)/n(H_2) so that HD is distributed rather uniformly throughout the model. At the lowest density, n(HD)/n(H_2) varies much less than the molecular fraction and the bulk of the HD resides near the center of the model.

Two effects directly attributable to dust extinction are shown in Figure 2. First, the n(HD)/n(H_2) ratio is slightly smaller in the outer regions of the models when dust attenuation is negelected, presumably because the attenuation by dust has a larger effect on HD than on H_2, given that HD is so much more weakly self-shielded. Second and most noticeably, the n(HD)/n(H_2) ratio does not rise near the center of models in which the extinction of dissociating photons by dust is neglected (but note that the scale in the upper panel of Figure 2 is much expanded compared to that at bottom). An analogous situation appears in Figure 1 for smaller values of ζ_H when N(HD) only rises sharply at N(H_2) $\gtrsim$ 10^{21} cm^{-2} in the presence of dust extinction. Although the H_2-fraction always reaches higher values toward the center of models when the explicit attenuation of dissociating photons by dust is included, sharp increases in n(HD)/n(H_2) and N(HD)/N(H_2) result primarily from the onset of strong HD self-shielding, triggered by the extinction due to dust. Whether the onset of H_2 self-shielding and high H_2-fractions is triggered by dust extinction is the subject of Section 4.

4. What triggers the onset of high H_2 and HD fractions?

4.1. The outermost self-shielding layer

In this work, dust extinction of dissociating photons is expressed using a single absorption cross-section $\sigma_d = 1.9\times10^{-21}N(H)$ as in the work of Draine & Bertoldi (1996) and Sternberg et al. (2014) and scattering is ignored. As shown in the Figure 2, dust extinction raises n(HD)/n(H_2) and f_{H_2} near the centers of the models but does not play a large role in triggering the onset of higher n(H_2) in the outer shielding layers except perhaps at the very lowest density: the curves showing the radial variation of f_{H_2} with and without dust extinction differ little in the outer radial

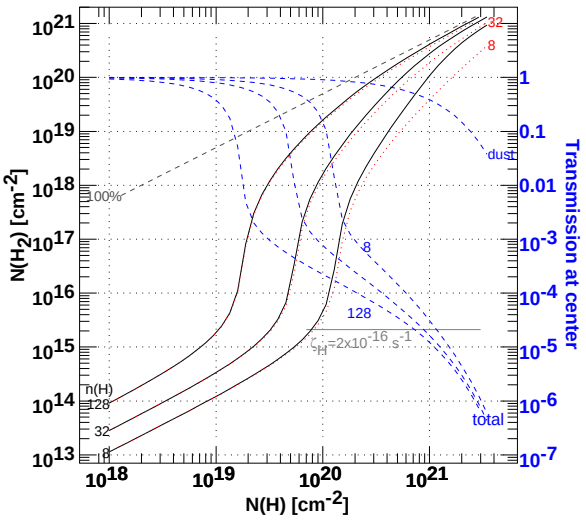

Fig. 3.— Calculated H_2 column densities and interior attenuations. The solid black curves represent the H_2 column density toward the geometric centers of models with n(H) = 8, 32 and 128 cm^{-3} over a wide range of cloud column density N(H) from front to back of the model, with $\zeta_H = 2 \times 10^{-16}$ s^{-1}. As in Figure 1 each solid curve has a dotted red companion representing the same model neglecting dust attenuation. Reading the scale at right, the blue dashed curves separately show the fraction of ambient H_2-dissociating photons that penetrates to the centers of the models after H_2 self-shielding and dust extinction (labelled "total") and the much smaller amount which the dust extinction contributed to that total. The grey horizontal line represents the attenuation at which the cosmic ray flux indicated becomes the dominant cause of H_2 destruction at the rate indicated.

regions where f_{H_2} abruptly increases by factors of 100 or more. The reason for this can be better understood in the context of Figure 3 showing the attenuation of dissociating photons in models with differing number and H_2 column density, along with the particular contribution from dust extinction of dissociating photons.

In Figure 3 the onset of higher H_2 fractions is scarcely affected by the presence of dust attenuation, rather, that is determined by the onset of strong H_2 self-shielding which already occurs at such small A_V that there is very little dust opacity even in the UV. If physical conditions foster small H_2-fractions at high N(H), the dust extinction and its effect on f_{H_2} may be appreciable for H_2 and this is the situation for HD as well at very high N(H) in Figure 1. The details depend on the slopes of the variation of the attenuation with column density: if the self-shielding of H_2 varies slowly with N(H_2), especially when f_{H_2} is larger, dust attenuation and small increases in N(H) may be efficient at increasing the molecular fraction locally. At the lowest number density in Figure 3, N(H_2) toward the center of the models about doubles for N(H) $\gtrsim 10^{21}$ cm^{-2} and the strong increases in HD were noted earlier. Whether clouds with such high N(H_2) exist at such low density is another matter.

Also shown in Figure 3 is the transmission at which the attenuation of the radiation field is so great that the destruction rate of H_2 by cosmic rays equals that due to photodissociation in the Lyman and Werner bands when $\zeta_H = 2 \times 10^{-16}$ s^{-1}. In fact the destruction of H_2 near the centers of our models is dominated by cosmic rays even for clouds having total A_V = 0.5 - 1 mag (see also Section 5.2). The high cosmic-ray ionization rates required to explain HD strongly limit the ability of dust extinction to increase f_{H_2} inside the outer self-shielding layer.

4.2. The overall contribution from dust extinction

The overall contribution of dust extinction of Lyman and Werner band photons is summarized in Figure 4 where for models with n(H) = 8, 16, ..., 128 cm^{-3} we show the total molecular fraction integrated over the model and the fraction of that total that is directly attributable to dust extinction, calculated symbolically as ((Mass with dust extinction)-(Mass without))/Mass(with). For conditions approximating a Spitzer Standard H I cloud with n(H) = 32 cm^{-3} and N(H)= 4×10^{20} cm^{-2} some 20% of the hydrogen is in H_2 and 30% of that is attributable to the presence of

dust extinction.

5. H_2 formation at Solar and sub-Solar metallicity

5.1. Observations

In Figure 5 we show N(H_2) and N(H) as determined in UV absorption in the Milky Way and the Magellanic Clouds. The galactic data include observations toward bright stars as studied by Copernicus (Savage et al. 1977) and toward bright stars (Rachford et al. 2002, 2009) and AGN (Gillmon & Shull 2006) using FUSE, extending to much higher N(H) than were available to Copernicus. The Southern Hemisphere data is from Tumlinson et al. (2002). The Milky Way data in this plot shows the familiar jump in N(H_2) at N(H) $\approx 2 - 5 \times 10^{20}$ cm^{-2} whereby the fraction of hydrogen in H_2 abruptly increases to ≥ 0.01.

Plotting N(H_2) against N(H) is unlike the situation shown in Figure 1, where sightlines have been ordered according to their H_2 column densities. Viewing the onset of H_2 formation along sightlines harboring a mixture of conditions involves several separate aspects of the ISM; the cold neutral medium of the ISM is clumped into diffuse "clouds" (usually called H I clouds by radio astronomers); H_2 forms in appreciable quantities in H I clouds having sufficiently high N(H); and lines of sight with N(H) $\gtrsim 3 \times 10^{20}$ cm^{-2} cross at least one of these clouds. The column densities at which the jump occurs has been increased, and somewhat spread out by the contribution from unrelated, less-molecular material along the line of sight, see Spitzer (1985).

The sightlines used by Gry et al. (2002) to determine R_G are marked in Figure 5; they all have very high H_2-fractions at their respective values of N(H): nonetheless the value of the grain surface H_2-formation rate constant derived in that work reproduces our temperature-dependent results extremely well as noted in Section 5.2 and as shown in Figure 6.

For the Large Magellanic Cloud (LMC), the metallicity is some 2.5 times smaller than that of the Milky Way (Z=0.007 vs. 0.018 (Dufour 1984)) and the jump in H_2 occurs around N(H) = 10^{21} cm^{-2}, roughly three times that of the Milky Way. According to Weingartner & Draine (2012) such N(H) corresponds to $A_V \approx$ 0.12 mag, as against A_V = 0.16 mag in the Milky Way. For the Small Magellanic Cloud (SMC) with Z = 0.002 (Dufour 1984), the jump in H_2 occurs at even higher N(H) $\approx 3 \times 10^{21}$ cm^{-2}, but corresponding to A_V = 0.18 mag (Weingartner & Draine 2012), again very similar to the Milky Way.

5.2. Modelling the onset of H_2 self-shielding

In Section 5.1 we showed that the surface area of large grains (as represented by A_V in the small range 0.12 mag $\lesssim A_V \lesssim$ 0.18 mag) is very nearly constant at the onset of strong self-shielding in H_2 in three systems of different metallicity, in principle leading to the question whether it is the extinction by these grains or their aggregate H_2-catalytic grain surface area that is responsible for the increase in the H_2-fraction with N(H).

The behaviour seen in Figure 3 suggests that only the grain catalytic area is important, because the dust extinction *per se* is small at the onset of H_2 self-shielding. This is further illustrated in Figure 6 showing the results of varying several parameters in models with n(H) = 32 cm^{-3}. This is the density of a Spitzer H I cloud and for typical ISM pressures p/k = $2 - 3000$ cm^{-3} K (Jenkins & Tripp 2011) it is consistent with the kinetic temperatures that have been inferred from the J=1 and J=0 levels of H_2, ie 77 K for the original Copernicus survey (Savage et al. 1977), 86 ± 20K and 124 ± 8K for FUSE sightlines toward distant AGN in the galactic disk and halo, respectively (Gillmon & Shull 2006) and 67 ± 15K for the highest column density translucent FUSE sightlines toward bright stars (Rachford et al. 2002, 2009). The kinetic temperatures in our models are in the range 50 - 160 K, varying inversely with n(H) and having somewhat higher pressure at higher density, as is generally the case for phase diagrams in multi-phase models of the diffuse ISM. This is all consistent with the heating-cooling model that we adopted and is discussed in greater detail by Wolfire et al. (2003).

The curves shown in Figure 6 cluster in two groups according to whether the H-H_2 transition is shifted appreciably. Some parameters have little effect. Replacing our temperature-dependent H_2 formation rate by the value derived by Gry et al. (2002) has little effect. Increasing the cosmic-ray ionization rate to $\zeta_H = 10^{-15}$ s^{-1} increases H_2 formation and hastens the onset of H_2 self-shielding at small N(H) because the models are somewhat warmer but H_2 formation is suppressed at the very highest N(H) because cosmic ray ionization so greatly dominates the H_2 destruction. The column density at the onset of H_2 self-shielding

Table 1: HD in high-z DLA and sub-DLA systems

Source	$Z/Z_\odot$	z	N(H I) log cm^{-2}	N(H_2) log cm^{-2}	N(HD) log cm^{-2}	2N(H_2)/N(H I)	N(HD)/N(H_2) /[D/H]	HD Ref.
Q1232	0.04	2.34	20.90(0.08)	19.68(0.08)	15.43(0.15)	0.121	2.21	1
Q1331a	0.04	1.78	21.20(0.04)[b]	19.43(0.10)	14.83(0.15)	0.034	0.99	2
Q1331b				19.39(0.11)	14.61(0.20)	0.031	0.65	2
FJ0812a	$\lesssim$0.36[a]	2.63	21.35(0.10)	19.93(0.04)	15.71(0.07)	0.076	2.37	2
FJ0812b			21.35(0.10)	18.82(0.37)	12.98(0.22)	0.006	0.06	2
J2123	0.5	2.06	19.18(0.15)	17.64(0.15)	13.84(0.20)	0.058	6.20	3
J1439	1	2.42	20.10(0.10)	19.38(0.10)	14.87(0.03)	0.380	1.22	4
J1237	2	2.69	20.00(0.15)	19.21(0.13)	14.48(0.05)	0.324	0.73	5

[a] Prochaska et al. (2003); Balashev et al. (2010)

[b] Prochaska & Wolfe (1999)

References (1) Ivanchik et al. (2010); (2) Balashev et al. (2010); (3) Tumlinson et al. (2010); (4) Noterdaeme et al. (2008); (5) Noterdaeme et al. (2010)

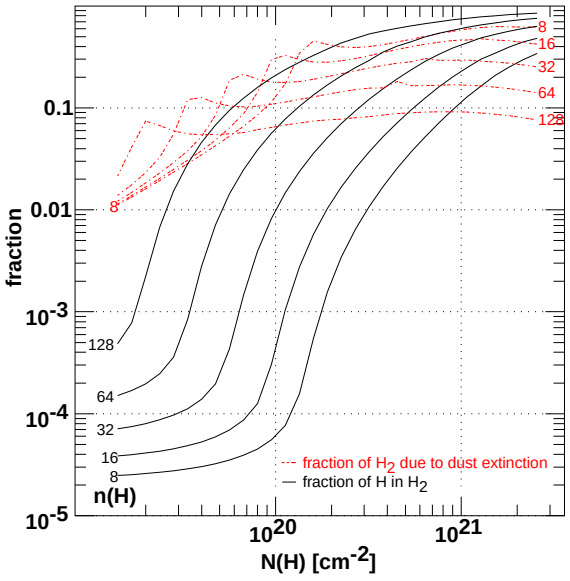

Fig. 4.— Molecular mass fractions and fractions of the molecular mass attributable to dust extinction. The solid curves show the fraction of the cloud model mass that is molecular at the indicated number and column density. The dash-dotted red curves nearer the top of the plot show the fraction of the molecular mass that is attributable to dust extinction of Lyman and Werner Band photons as discussed in Section 4.

scales inversely with the radiation field as expected from the discussion in Appendix B but dependence on the radiation field is extremely complex because the thermal and ionization balance is strongly affected. Stronger radiation heats the models, increasing the H_2 formation rate, somewhat compensating the increased photodissociation.

Also shown in Figure 6 are curves corresponding to decreasing the grain surface H_2-formation rate constant R_G by a factor of 10, and separately, a calculation depleting the quantity of large, H_2-forming grains by the same amount and perforce also lessening the extinction by dust of dissociating photons by the same amount. Figure 6 shows that the onset of H_2 self-shielding in the outer shielding layer depends linearly on the grain surface area, but only to the extent that this area is available for catalytic H_2 formation; reducing the grain formation rate and the surface area of large grains both result in self-shielding at very nearly the same N(H), confirming that the extinction provided by the grain surface area is a small effect on the initial onset of strong H_2 self-shielding and the H I - H_2 transition.

The effects directly attributable to the grain surface area differ noticeably inside the self-shielding layer. When large grains are removed entirely the H_2-fraction does not exceed 10% except at very large N(H), which is the case in Figure 5 for the sightlines with sub-Solar metallicity. Inside the self-shielding layer, dust extinction drives the H_2-fraction higher, and dust extinction will have a strong effect whenever the H_2 fraction is substantially below unity well inside the outer

self-shielding layer; this would be the case at low n(H) and large N(H) if those conditions actually occur in the ISM. This has interesting consequences for the time-evolution of the H_2 fraction, because regions with lower molecular fraction equilibrate earlier, and, even though dust extinction can increase the equilibrium molecular fraction inside the self-shielding layer, it does not hasten the approach to equilibrium. When dust extinction matters to the H_2 fraction the times to reach H_2 equilibrium will be long.

6. HD formation at high redhshift and/or low metallicity

The observations of HD in DLA and sub-DLA systems at high redshift are summarized in Table 1 and shown in Figures 1 and 7. Although DLA and sub-DLA systems typically have low metallicity, the systems in which HD has been detected cover a wide range of metallicity from $Z/Z_\odot$= 0.04 to 2. It is relatively easy to explain the high N(HD)/N(H_2) seen at high z in terms of higher density when the metallicity is small and rather puzzling that the high redshift systems are so similar in having such high HD/H_2 ratios while the metallicity varies over such a wide range.

Figure 6 shows that a given N(H_2) will be seen at smaller molecular fractions in systems of lower metallicity because the required N(H) is larger; indeed, the DLA and sub-DLA systems at high redshift have comparable N(HD) to those seen in the Milky Way sightlines, but generally at smaller molecular fractions overall. In Table 1 systems with high and low metallicity have comparable values of N(H_2) but with much smaller f_{H_2} at the low-metallicity end.

Unlike the case at Solar metallicity illustrated in Figure 1 where N(HD)/N(H_2) decreases with density, larger proton densities and higher HD/H_2 ratios are expected at *higher* number density when the metallicity is small. Higher proton densities are always more readily available in principle at higher number densities but radiative recombination with electrons from ionized carbon and neutralizations by small grains suppress the proton fraction at higher density when the metallicity is near-Solar. When the metallicity is small, the effects of both electrons and small grains are sharply curtailed and the proton density better tracks the number density overall.

The situation is illustrated in Figure 7 where we varied the metallicity in our calculations by linearly scaling the abundance of all metals or metal-bearing

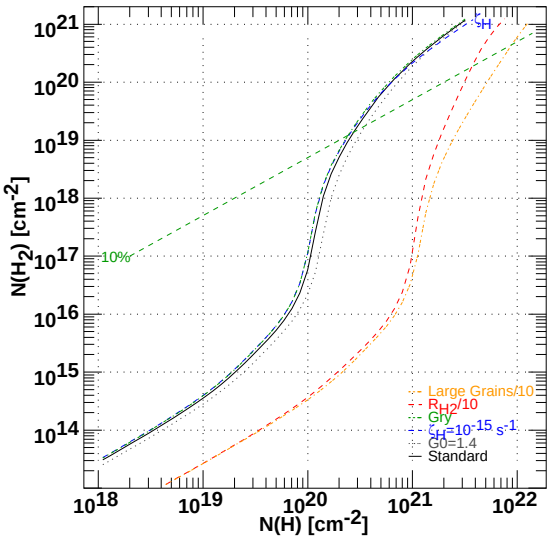

Fig. 6.— Other influences on N(H_2) for models at n(H) = 32 cm^{-3}. The group of curves at the left includes a "standard" model (solid black), a model with the radiation field increased by 40% (dotted grey), a model using the temperature-independent H_2-formation rate of Gry et al. (2002) (dash-dot green) and a model with $\zeta_{H_2} = 10^{-15}$ s^{-1} (dashed, blue). At right are models with a diminished grain formation rate coefficient (dashed red) and a model in which 90% of the large grains are entirely removed from the calculation (dash-dot orange). The green dashed line indicates the locus where 10% of the hydrogen is in molecular form. These models were computed along sightlines displaced 5/6 of the radius from the center, compare with Figure 3 to see that the H I - H_2 transition has been displaced toward higher N(H) compared with models observed through the central sightline.

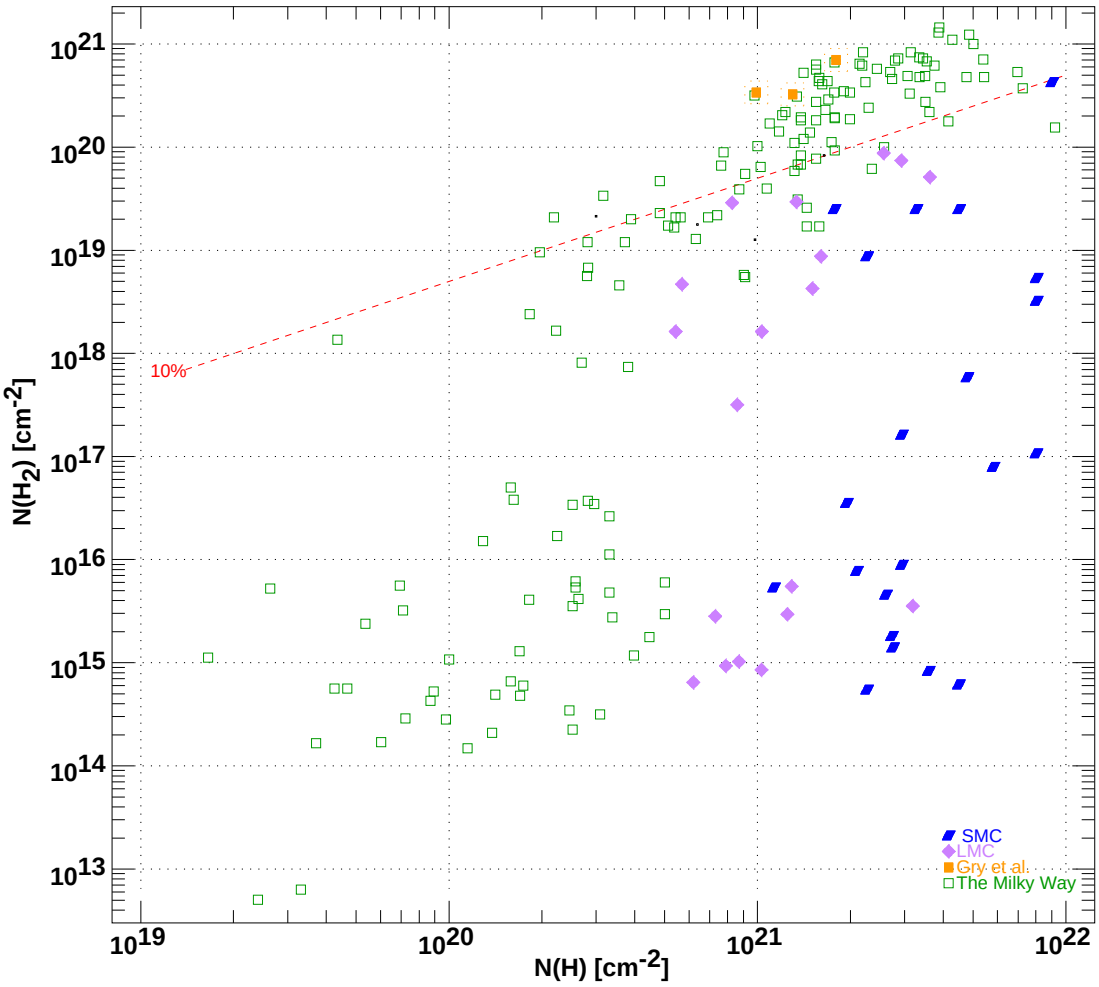

Fig. 5.— H_2 column densities for the Milky Way and Magellanic Clouds. The Milky Way data include results from Savage et al. (1977), Rachford et al. (2002) and Gillmon & Shull (2006) and are shown as open green rectangles; the three lines of sight used by Gry et al. (2002) to determine the H_2-formation rate coefficient are separately marked. Results for the SMC and LMC are taken from Tumlinson et al. (2002).

species (ie the large and small dust grains). At left it is shown that the N(HD)/N(H_2) ratio increases at least as fast as 1/Z at n(H) = 128 cm^{-3} in the range of N(H_2) where HD is observed at high redshift. At right in Figure 7 the increase of N(HD)/N(H_2) with density is shown for $Z/Z_\odot$= 1/16. The functional dependence on density is weaker than linear but the senseis quite contrary to the variation with density shown in Figure 1 at Solar metallicity.

6.1. n(H) inferred for J0812+3208A

Balashev et al. (2010) derived T_K = 48 ± 2 K from comparison of the J=1 and J=0 levels of H_2 toward J0812+3208A and observed a ratio log N_1/N_0 = -1.93 in the J=1 and J=0 levels of HD. Unlike H_2 the J=1-0 transition of HD is permitted, with a small dipole moment and a spontaneous transition rate A_{10} = 5.1 × 10^{-8} s^{-1} (Flower et al. 2000). Balashev et al. (2010) pointed out that the HD level populations can be used to derive the ambient density and they quote n ≈ 50 cm^{-3} using a two-level atom approach under the assumption that radiative pumping of the J=1 level is negligible. They made several errors in their discussion, most importantly using the downward collision rate C_{10} in their unnumbered expression for the number density (their Section 3.2) when the smaller upward rate is actually called for.

The collisional rate constants for HD excitation by H, He, and H_2 are given by Flower et al. (2000). They allow a number of important simplifications in the analysis below 100 K, because the rate constants are the same for H and He, and the same for ortho- and para-H_2. As well the rate for H_2 excitation is just twice that for atomic hydrogen so that the analysis is independent of the molecular fraction. Denoting the upward rate constant for excitation by atomic hydrogen as C_{01} and the spontaneous emission coefficient as A_{10}, the total hydrogen number density may be written as

$$n(H) = \frac{N_1}{N_0}\frac{A_{10}}{C_{01}} \times \frac{1}{1 + [\mathrm{He/H}]}$$

$$C_{01} = \frac{g_1}{g_0} e^{-E_{10}/kT_K} C_{10} = 3e^{-128/T_K} C_{10}$$

$$C_{10} = 3.2 \times 10^{-12} \mathrm{cm^3\ s^{-1}} T_K^{1/3}$$

in the limit of weak excitation n(H)C_{01} << A_{10}.

With T_K = 48K and [He]/[H] = 0.085 by number, we find n(H) = 240 cm^{-3}. Such a density is consistent with observed, relatively high HD/H_2 at low metallicity (Figure 7) and indeed Balashev et al. (2010) considered that log $Z/Z_\odot$= -1. However Prochaska et al. (2003) actually derived [O]/[H] ≈ 0.36 Solar and similar results for [Zn]/[H], so that J0812 is *not* an especially low-metallicity system.

7. Summary

7.1. HD

In Section 3 (see Figure 1) we showed that the ratios N(HD)/N(H_2) ≈ 3 × 10^{-6} in the Milky Way are primarily diagnostic of the cosmic-ray ionization rate and secondarily of the number density in the sense of ζ_H/n(H) tending to be constant, with 16 cm^{-3} ≲ n(H) ≲ 128 cm^{-3} for $\zeta_H = 2\times10^{-16}$ s^{-1}. The gas sampled in galactic HD measurements has moderate density and molecular fraction $f_{H_2} \approx 0.1 - 0.5$, because the proton densities necessary to ensure adequate protonation are more difficult to maintain at the higher densities that are more favorable to H_2 formation overall (see Figures 2 and 8).

In Section bf 6 we discussed N(HD) and N(H_2) observed in high-redshift DLA and sub-DLA systems. DLA and sub-DLA systems observed at z > 1.7 have much higher N(HD)/N(H_2) ratios compared to the Milky Way, ie with comparable N(HD) but order of magnitude smaller N(H_2) and somewhat smaller N(H_2)/N(H I). In Section 5 (Figure 5) we discussed how smaller H_2 fractions are observed in nearby systems with sub-Solar metallicity: H_2 becomes self-shielding at progressively larger N(H I) and smaller H_2 fractions, but with nearly-fixed A_V = 0.15 ± 0.03 mag when comparing the Milky Way and Magellanic Clouds (Figure 5). In Section 5 (see Figure 6) we showed that the onset of H_2 self-shielding at progressively higher N(H I) and fixed A_V is a consequence of the smaller dust/gas ratio at smaller metallicity, and the consequent smaller grain surface area per unit hydrogen that is available for H_2 formation.

In Section 6 (see Figure 7) we showed that higher N(HD)/N(H_2) and smaller N(H_2)/N(H) can be explained at higher density in systems of smaller metallicity, because the proton density increases with increasing number density, opposite to the Milky Way case at Solar metallicity. Moreover, in one case where the J=1 level of HD is observed in a high-redshift system, the derived number density n(H) ≈ 240 cm^{-3} is relatively high. However this system is not obviously of very low metallicity (Z/Z_{Solar} ≲ 0.36) and

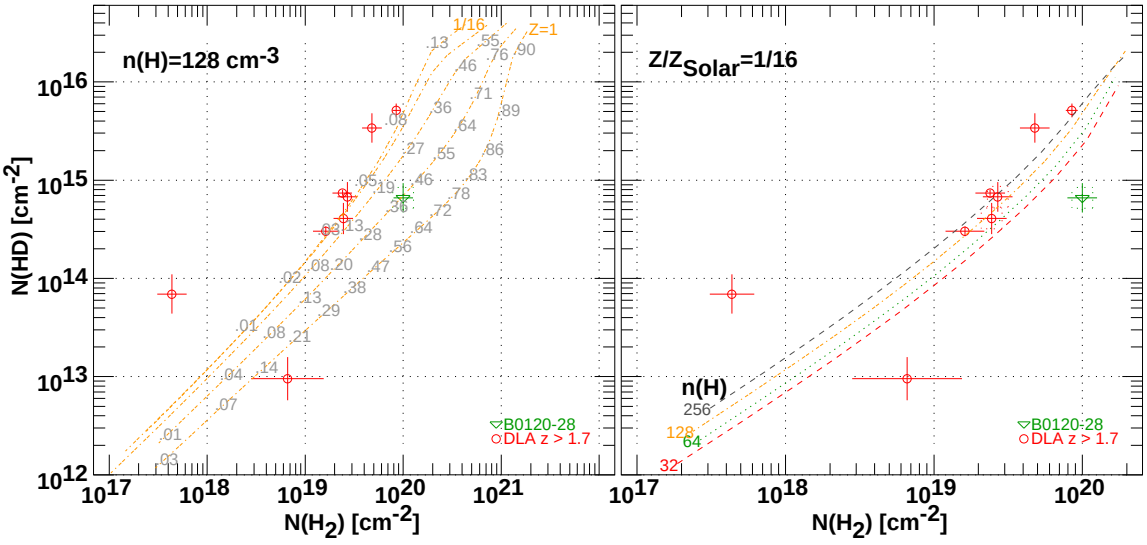

Fig. 7.— Influence of density and metallicity on N(HD)/N(H_2). Left: at n(H) = 128 cm^{-3} the metallicity is varied in steps of two from Solar to 1/16 Solar. Values of f_{H_2} are indicated in gray along the curves. Right:n(H) is varied in steps of two over the range 32 cm^{-3} ≤ n(H) ≤ 256 cm^{-3} at 1/16 Solar metallicity.

high N(HD)/N(H_2) ratios ranging from 80-200% of the cosmic [D/H] are observed in high redshift systems over a wide range of metallicity ranging from 0.04 to 2 times Solar (Table 1) for the 6 out of 8 high z systems with N(H_2) > 8×10^{19} cm^{-2} and smaller quoted column density errors. Conversely, a low-redshift DLA system at z = 0.18 has N(HD) and N(H_2) values typical of Milky Way gas and a high H_2 fraction, but at metallicity only 7% Solar.

It seems odd that the high-redshift systems should share such high N(HD)/N(H_2) values while having so little else in common in terms of the fractionation chemistry expected at their quoted metallicities. For the high-z systems it is tempting to abandon the fractionation scenario, with its implication of a high H-ionization rate, in favor of an ad hoc scenario in which the molecules are in some tight knot where the conversion of both hydrogen and deuterium to molecular form is nearly complete. But this begs the question of why such similar and unusual conditions would exist over such a wide range of metallicity.

7.2. H_2 and the effect of dust extinction

Motivated by effects like the sharp central upturns in HD/H_2 observed in the upper panel of Figure 2, or as seen in Figure 1 at smaller ζ_H and high N(H_2), we broke out the explicit extinction of H_2-dissociating Lyman and Werner Band photons by dust. As shown in Figures 2 and 3 and discussed in Sections 3 and 4, the outer self-shielding layer in H_2 is just that, triggered by non-linear effects inherent in the cross-section for H_2 photo-absorption (Figure 3) with little dependence on the existence of extinction by dust. Only at very small n(H) in a regime that is probably not thermally stable in two-phase ISM is the location of the onset of H_2-self shielding appreciably shifted by dust extinction.

By contrast, there is a somewhat wider range of number density where dust extinction has an appreciable effect on the H_2 fraction inside the outermost H_2 self-shielding layer. As shown in Figure 4, about one-third of the H_2 in a cloud at n(H) = 32 cm^{-3} is directly attributable to dust extinction.

The effects of dust extinction on HD are somewhat greater owing to its lesser degree of self-shielding. As shown in Figure 2, HD/H_2 ratios are increased slightly even in the outer portions of our models, with much stronger effects toward the center and even moreso at lower density. Increases in either the amount of H_2 or the attenuation of HD-dissociating photons can tip the HD over into a non-linear regime where its local abundance is strongly dependent on its own self-shielding and somewhat less on the local fractionation chemistry.

In discussing the dependence of H_2 formation on

metallicity, Figure 5 shows how the location of the onset of strong H_2 self-shielding shifts monotonically to higher N(H) with decreasing metallicity, in such a way as to keep constant the inferred A_V representing the total column of grain surface area, see Sections 5 and 6. This constancy of A_V could be interpreted as implying that the onset of H_2 self-shielding is caused by the extinction due to dust, but that is not the case. As shown in Figure 6, it is the lessening of the grain surface area available for H_2 formation that causes the shift, while the dust extinction *per se* increases the H_2 fraction at yet-higher N(H), inside the H_2 self-shielding layer. As shown in Figure 6, producing H_2 fractions above 10% requires even much higher N(H) in low-metallicity systems owing to the diminished dust extinction cross section per H-atom.

The National Radio Astronomy Observatory is currently operated by Associated Universities, Inc. under a cooperative agreement with the National Science Foundation. The hospitality of the ITU-R and Hotel Bel Esperance in Geneva and the UKATC and the Apex City Hotel in Edinburgh are appreciated during the writing of this manuscript.

A. Intra-cloud variation of the proton and electron densities

Evaluating Eq 1 we find n(p) $\approx$ 0.004 cm^{-3} for T = 75 K, using the photodissociation rate of HD $\Gamma_{HD} = \Gamma_{H_2} = 4.3 \times 10^{-11}$ s^{-1} in free space (Draine & Bertoldi 1996) and N(HD)/N(H_2) $\approx 3 \times 10^{-6}$ as shown in Figure 1. This can be compared with the results shown in Figure 8, where we have plotted the proton and electron densities just inside the outer edge and at the center of the models whose results were depicted in Figure 1.

The electron and proton densities behave very differently with respect to changes in density, largely because carbon remains ionized under all conditions, putting a floor on n(e) that does not exist for n(p). At the outer edge, n(e) increases with density while n(p) remains nearly fixed owing to a balance between the volume ionization n(H) ζ_H and the neutralization by small grains, whose density and neutralization rate change in fixed proportion to n(H). The electron density decreases toward the centers of all the models because the ionization fraction due to ionized hydrogen (ie, n(p)) decreases there. The proton density decreases by nearly the same factor at all density while the decrease in the electron density at the center is small at high density when ionization of hydrogen is weak.

The decline of n(p) toward the cloud center means that the chemistry has an innate tendency to segregate protons and H_2, shown in Figure 2, complicating the HD formation problem. In Section 3.3 we noted that the distribution of HD is more uniform in radius at higher density, and the models have higher f_{H_2} at higher n(H) but overall it is the proton density that is decisive, and Figure 1 shows that lower density clearly wins the HD battle at Solar metallicity.

B. Scaling parameters for the H_2-formation problem

Simply writing down the equation for the growth of H_2

$$dn(\mathrm{H_2})/dt = -n(\mathrm{H_2})\Gamma_{\mathrm{H_2}} + \mathrm{R_G} n(H) n(HI) \sqrt{T_K} \quad (1)$$

and setting dn(H_2)/dt = 0 to achieve a formal solution (formal because n(H) = n(H I) + 2n(H_2) and Γ_{H_2} is functionally dependent on N(H_2))

$$n(\mathrm{H_2})/n(HI) = \mathrm{R_G} \sqrt{T_K} n(H)/\Gamma_{\mathrm{H_2}}$$

shows that $\Gamma_{H_2}/(\mathrm{R_G} n(H) \sqrt{T_K})$, the n($H_2$)/n(H I) ratio in free-space, is a dimensionless scaling parameter for this problem. It serves as the basis of the discussion of Federman et al. (1979) who in terms of our quantities defined $1/\epsilon$ = n(H I)/2n(H_2) = $\Gamma_{H_2}/(2\mathrm{R_G} n(H) \sqrt{T_K})$ and showed that the data of Savage et al. (1977) (see Figure 6 here) could be reproduced with $\epsilon = 6 \times 10^{-5}$ corresponding to n(H) $\approx$ 33 cm^{-3} for $\mathrm{R_G} \sqrt{T_K} = 3.9 \times 10^{-17}$ cm^{-3} (Gry et al. 2002) and $\Gamma_{H_2} = 4.3 \times 10^{-11}$ s^{-1}. The formulation by Federman et al. (1979) does not consider shielding due to dust and indeed, our models showed that dust shielding contributes modestly at that density at Solar metallicity (Section 4.2). The formulation of Federman et al. (1979) is numerically intensive but it provides a description of the width and location of the self-shielding layer without additional assumptions because the equilibrium conditions are solved exactly, although not analytically.

The effects of dust extinction, shown in many instances in our models but most important at small n(H), were incorporated in the analytic formulation of Sternberg and his collaborators (Sternberg 1988; Sternberg et al. 2014) whose most recent description defines parameters $\alpha = 2/\epsilon$ and G that is the mean H_2 self-shielding factor including the dust-extinction associated with N(H_2) (ie, not N(H)). The total dust column is considered to have two parts, called the H I and H_2 dust, whose columns are proportional to N(H I) and N(H_2). In this formulation the structure of the H I - H_2 transition is determined by the product αG. The αG << 1 and αG >> 1 limits are called the weak- and strong field limits, respectively. The domain where αG $\approx$ 1 marks the transition between H I and H_2-dominated regimes as indeed seen from the basic definition of α or ϵ as H I/H_2 ratios; one replaces the small free-space H_2/H I ratio by that in the strongly shielded transition zone. In effect, our models lie in the transition between two regimes, as understood in the context of the underlying physics of the heating, cooling and ionization balance.

Krumholz et al. (2008) explicitly introduced the total attenuation due to dust into the equation of detailed balance (akin to eqn 1), resulting in the creation of a hybrid (chimerical?) parameter χ that is in effect a redefinition of $1/\epsilon$.

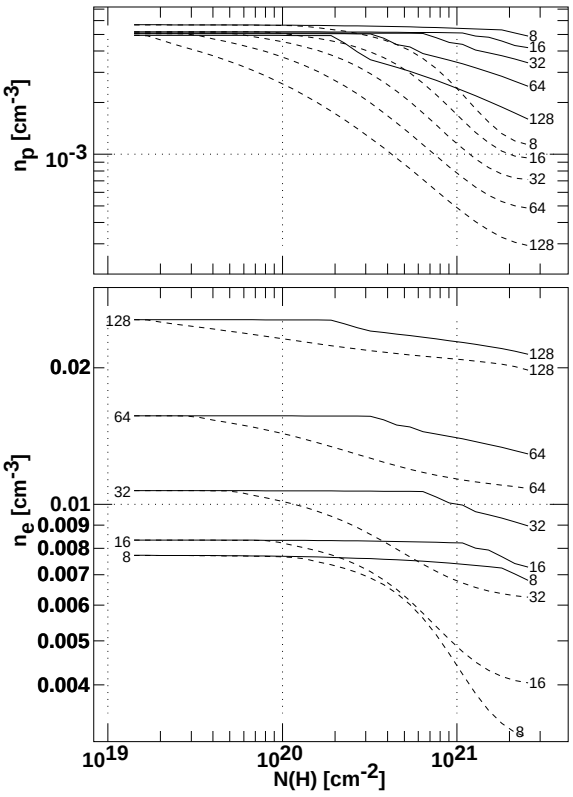

Fig. 8.— Proton (upper) and electron densities for some of the models employed in Figure 1. The solid lines are for locations just inside the outer edge of the models; the dashed lines are at the center. In all cases the primary cosmic ray ionization rate per H-atom is $\zeta_H = 2 \times 10^{-16}$ s^{-1}. The electron and proton densities move oppositely in response to changes in density at solar metallicity, see Section 7.

In χ, the H_2 photoabsorption cross section that determines Γ_{H_2} is replaced by the cross-section for dust extinction. Because the dust cross section is so much smaller, one deals with χ-values of order unity in the H I - transition region as with Sternberg's formulation. Sternberg et al. (2014) show that $\chi = \alpha G$ in the limit of low metallicity.

REFERENCES

Bakes, E. L. O. & Tielens, A. G. G. M. 1994, ApJ, 427, 822

Balashev, S. A., Ivanchik, A. V., & Varshalovich, D. A. 2010, Astronomy Letters, 36, 761

Black, J. H. & Dalgarno, A. 1973, ApJ, 184, L101

Cooke, R. J., Pettini, M., Jorgenson, R. A., Murphy, M. T., & Steidel, C. C. 2014, ApJ, 781, 31

Draine, B. T. 2003, Ann. Rev. Astrophys. Astron., 41, 241

Draine, B. T. & Bertoldi, F. 1996, ApJ, 468, 269

Draine, B. T. & Sutin, B. 1987, ApJ, 320, 803

Dufour, R. J. 1984, in IAU Symposium, Vol. 108, Structure and Evolution of the Magellanic Clouds, ed. S. van den Bergh & K. S. D. de Boer, 353–360

Federman, S. R., Glassgold, A. E., & Kwan, J. 1979, ApJ, 227, 466

Flower, D. R., Le Bourlot, J., Pineau des Forêts, G., & Roueff, E. 2000, Mon. Not. R. Astron. Soc., 314, 753

Gay, C. D., Stancil, P. C., Lepp, S., & Dalgarno, A. 2011, ApJ, 737, 44

Gillmon, K. & Shull, J. M. 2006, ApJ, 636, 908

Gry, C., Boulanger, F., Nehmé, C., Pineau des Forêts, G., Habart, E., & Falgarone, E. 2002, A&A, 391, 675

Hollenbach, D., Kaufman, M. J., Neufeld, D., Wolfire, M., & Goicoechea, J. R. 2012, ApJ, 754, 105

Indriolo, N., Neufeld, D. A., Gerin, M., Geballe, T. R., Black, J. H., Menten, K. M., & Goicoechea, J. R. 2012, ApJ, 758, 83

Ivanchik, A. V., Petitjean, P., Balashev, S. A., Srianand, R., Varshalovich, D. A., Ledoux, C., & Noterdaeme, P. 2010, Mon. Not. R. Astron. Soc., 404, 1583

Jenkins, E. B. & Tripp, T. M. 2011, ApJ, 734, 65

Jura, M. 1974, ApJ, 191, 375

Krumholz, M. R., McKee, C. F., & Tumlinson, J. 2008, ApJ, 689, 865

Lacour, S., André, M. K., Sonnentrucker, P., Le Petit, F., Welty, D. E., Desert, J.-M., Ferlet, R., Roueff, E., & York, D. G. 2005, A&A, 430, 967

Le Petit, F., Roueff, E., & Le Bourlot, J. 2002, A&A, 390, 369

Lee, H. H., Herbst, E., Pineau Des Forets, G., Roueff, E., & Le Bourlot, J. 1996, A&A, 311, 690

Linsky, J. L., Draine, B. T., Moos, H. W., Jenkins, E. B., Wood, B. E., Oliveira, C., Blair, W. P., Friedman, S. D., Gry, C., Knauth, D., Kruk, J. W., Lacour, S., Lehner, N., Redfield, S., Shull, J. M., Sonneborn, G., & Williger, G. M. 2006, ApJ, 647, 1106

Liszt, H. 2003, A&A, 398, 621

Liszt, H. S. 2006, A&A, 452, 269

—. 2007, A&A, 461, 205

McCall, B. J., Hinkle, K. H., Geballe, T. R., Moriarty-Schieven, G. H., Evans, N. J., Kawaguchi, K., Takano, S., Smith, V. V., & Oka, T. 2002, ApJ, 567, 391

Noterdaeme, P., Petitjean, P., Ledoux, C., López, S., Srianand, R., & Vergani, S. D. 2010, A&A, 523, A80

Noterdaeme, P., Petitjean, P., Ledoux, C., Srianand, R., & Ivanchik, A. 2008, A&A, 491, 397

O'Donnell, E. & Watson, W. D. 1974, ApJ, 191, 89

Oliveira, C. M., Sembach, K. R., Tumlinson, J., O'Meara, J., & Thom, C. 2014, ApJ, 783, 22

Pettini, M. & Cooke, R. 2012, Mon. Not. R. Astron. Soc., 425, 2477

Prochaska, J. X., Howk, J. C., & Wolfe, A. M. 2003, Nature, 423, 57

Prochaska, J. X. & Wolfe, A. M. 1999, Astrophys. J., Suppl. Ser., 121, 369

Rachford, B. L., Snow, T. P., Destree, J. D., Ross, T. L., Ferlet, R., Friedman, S. D., Gry, C., Jenkins, E. B., Morton, D. C., Savage, B. D., Shull, J. M., Sonnentrucker, P., Tumlinson, J., Vidal-Madjar, A., Welty, D. E., & York, D. G. 2009, Astrophys. J., Suppl. Ser., 180, 125

Rachford, B. L., Snow, T. P., Tumlinson, J., Shull, J. M., Blair, W. P., Ferlet, R., Friedman, S. D., Gry, C., Jenkins, E. B., Morton, D. C., Savage, B. D., Sonnentrucker, P., Vidal-Madjar, A., Welty, D. E., & York, D. G. 2002, ApJ, 577, 221

Savage, B. D., Drake, J. F., Budich, W., & Bohlin, R. C. 1977, ApJ, 216, 291

Snow, T. P., Ross, T. L., Destree, J. D., Drosback, M. M., Jensen, A. G., Rachford, B. L., Sonnentrucker, P., & Ferlet, R. 2008, ApJ, 688, 1124

Spitzer, L. 1978, Physical processes in the interstellar medium (New York Wiley-Interscience, 1978. 333 p.)

Spitzer, Jr., L. 1985, ApJ, 290, L21

Stancil, P. C., Lepp, S., & Dalgarno, A. 1998, Astrophysics, 509, 1

Sternberg, A. 1988, ApJ, 332, 400

Sternberg, A., Le Petit, F., Roueff, E., & Le Bourlot, J. 2014, ApJ, 790, 10

Tumlinson, J., Malec, A. L., Carswell, R. F., Murphy, M. T., Buning, R., Milutinovic, N., Ellison, S. L., Prochaska, J. X., Jorgenson, R. A., Ubachs, W., & Wolfe, A. M. 2010, ApJ, 718, L156

Tumlinson, J., Shull, J. M., Rachford, B. L., Browning, M. K., Snow, T. P., Fullerton, A. W., Jenkins, E. B., Savage, B. D., Crowther, P. A., Moos, H. W., Sembach, K. R., Sonneborn, G., & York, D. G. 2002, ApJ, 566, 857

Watson, W. D. 1973, ApJ, 182, L73

Weingartner, J. C. & Draine, B. T. 2012, ApJ, 745, 173

Wolfire, M. G., Hollenbach, D., McKee, C. F., Tielens, A. G. G. M., & Bakes, E. L. O. 1995, ApJ, 443, 152

Wolfire, M. G., McKee, C. F., Hollenbach, D., & Tielens, A. G. G. M. 2003, ApJ, 587, 278

This 2-column preprint was prepared with the AAS LaTeX macros v5.2.